Modeling of Artificial Snow Production Using Annular twin-fluid nozzle

Malene Nordbø[1]   Odd Ivar Lindløv[2]   Joachim Lundberg[1]

[1]Department of Process, Energy and Environmental Technology, University of South-Eastern Norway, Norway,
`Joachim.lundberg@usn.no`
[2]Nedsnødd AS, Norway

Abstract

Nedsnødd AS develops a system for generating artificial snow. The concept is to optimize snow production for geographical locations where so-called 'marginal' conditions for snow production dominate the weather picture. To produce artificial snow, liquid water in a spray is exposed to cold air and becomes an agglomerate of frozen droplets. The basic idea is to improve the atomization of water to enhance the snow production capability. This work develops a model for the cooling process of the water droplets to simulate the processes determining the capabilities for snow production equipment.

Keywords: heat transfer, mass transfer, droplets

1   Introduction

Nedsnødd AS is a company specialized in nozzles for artificial snow production in climatically marginal regions. Marginal conditions mean that the climate is close to 0°C and the humidity is high. To produce artificial snow, liquid water is discharged as a spray to cold air and becomes an agglomerate of frozen droplets.

The basic mechanism of natural snow generation is kernel growth, in contrast to artificial snow where multi-droplet agglomeration is dominant. The trajectory of natural snow is several orders of magnitude longer than artificial snow. Several factors affect the production of artificial snow: air temperature and humidity, water temperature and velocity, droplet size distribution, and possible amount of nucleation kernels to enhance growth.

Current equipment for snow production has the disadvantage of high energy consumption (Techno Alpin, 2021) and the tendency to produce too wet snow at marginal conditions. By enhancing water atomization, artificial snow is produced at reduced water and air pressures, which reduce the energy consumption and ultimately the cost of the snow.

The artificial snow production technology started in the 1940s by a mistake where Dr. Ray Ringer studied the effect of rime icing on a jet engine in Canada. In 1961, Alden Hanson designed and patented a so-called snow fan machine for the generation of artificial snow by the addition of nucleation agents. Later on, several inventors have developed snow machines based on developed technology in addition to trial-and-error tests (Bellis, 2020).

Today, artificial snowmaking products are available worldwide, but the theory behind technology and process is not well documented or published. For this study, datasheets from different vendors and experimental studies performed in the Austrian Alps (Olefs et al., 2010) and at NTNU (Berg, 2017) have been used to understand how artificial snow production technology works.

Olefs et al. (2010) investigated the maximum wet-bulb temperature for producing artificial snow in the Alps. The study's author recommends that the maximum air temperature for producing snow is -1°C with 75% relative humidity but do not specify what weather conditions resulted in the snow density of 400 kg/m^3. They also indicated that relative humidity plays an essential role in the freezing process, where the amount of cooling is directly proportional to the relative humidity. If the humidity decrease, the evaporative cooling increases which give better snowmaking conditions.

Berg (2017) investigated techniques for artificial snow production aimed at Granåsen ski resort with an altitude of 180 m in Trondheim, which is in marginal conditions. The equipment of the study is a Northwind 450 snow fan, produced by DemacLenco with a water pressure of 30 bar(g). The estimate for the production of artificial snow was 52 m^3/h of snow. The lowest snow-density was found to be 811-936 kg/m^3. The study was performed in March, but ambient relative humidity and temperature are not specified.

Current work uses a novel twin-fluid nozzle developed by Nedsnødd AS. The nozzle is applied to a lance using low pressure (<5 bar(g)) air and water. An expanding air jet is aimed onto a deflector plate where an annular water sheet meets the high-velocity air jet. The result is enhanced droplet breakup and the droplets are expected to be smaller than for traditionally flat fan sprays. The nozzle design is similar to Lundberg et al. (2019).

A model is developed to simulate the behavior of the Nedsnødd artificial snow nozzle and the outcomes are discussed. The model is supported by experimental measurements. An image of the setup for the artificial snow spray is given in Figure 1.

Figure 1. Experimental setup and artificial snow spray located in Arabygdi.

2 Materials and methods

Artificial snow consists of cold small water droplets, that stick together to make agglomerates of droplets to imitate natural snow. In this work, an annular sheet twin-fluid nozzle is used to generate the droplets (Figure 2). The nozzle utilizes compressed air to accelerate the flow through a venture-type nozzle aimed at an external deflection cone. An annular water sheet is exposed to the deflected high-velocity airflow. Due to the high velocity of the air, the water sheet breaks up into fine water droplets with a high initial velocity. Traveling from the nozzle the droplets are exposed to ambient air where both mass (evaporation) and heat (convection) transfer occur. Depending on the surrounding air temperature and relative humidity, the droplets may freeze or remain as a liquid until it reaches the ground.
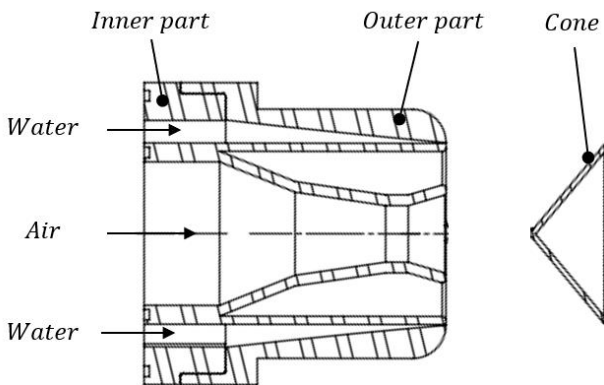
Figure 2. Split drawing of the Nedsnødd AS nozzle.

2.1 Modeling

The model is limited to single-sized droplets with ambient air at constant relative humidity, pressure, and temperature. In addition, the collision between the droplets throughout the trajectory and the interaction between other droplets are neglected. The models for atomization air from the nozzle, the water droplets, and the surrounding air are combined to output droplet behaviors like heat transfer, mass transfer, and droplet trajectory.

An important parameter in artificial snowmaking is relative humidity. It can be found by Cengel et al. (2015) using the vapor pressure of the water in the ambient air (P_v) divided by the saturation vapor pressure ($P_{v,sat@T}$) at the ambient pressure using:

$$RH\% = \frac{P_v}{P_{v,sat@T}} \quad (1)$$

The saturated vapor pressure is calculated using Buck's formula (Xu et al., 2012). It is assumed that the $RH\%$ is constant.

The velocity of the atomization air is modeled using thermodynamic relations for compressible flow (Cengel et al., 2015) as:

$$u_{a,0} = \sqrt{\gamma R_a T_{a,0}} \quad (2)$$

where γ, R_a, and $T_{a,0}$ is the heat capacity ratio, specific gas constant, and initial atomization air temperature, respectively.

The initial velocity of the water sheet is modeled using:

$$u_{sheet} = \frac{\dot{m}_w}{\rho_d A_{sheet}} \quad (3)$$

where

$$A_{sheet} = \frac{\pi}{4} \left((d_{annular} + \epsilon)^2 - d_{annular}^2 \right). \quad (4)$$

$d_{annular}$ is the internal diameter of the sheet and ϵ is the sheet thickness. $\dot{m}_w$ is the mass flow of water and ρ_d is the water or droplet density.

Using Equations 2 and 3 indicates the initial droplet velocity, nevertheless the air velocity is in the order of 300 m/s and the sheet in the order of 10 m/s. The droplets are assumed to have an initial velocity of 10% of the air velocity with the directional vector:

$$u_{d,x0} = 0.1 \cdot u_{a,0} \cos(\theta) \quad (5)$$

$$u_{d,y0} = 0.1 \cdot u_{a,0} \sin(\theta) \quad (6)$$

where the angle θ is the deflection angle of the cone.

The density of surrounding air is modeled as Tracy et al. (1980) like:

$$\rho_{amb} = \frac{P}{287.04(T_{amb} + 273.15)} \quad (7)$$

where P is the atmospheric pressure and T_{amb} is the ambient temperature.

2.1.1 Motion (droplet trajectory)

An expression for the trajectory is found by applying Newton's second law on a droplet, as shown in Figure 3. Here, the drag, gravity, and buoyancy forces are included. Notice that if the drag force is equal to the gravity force, the acceleration becomes zero, gives the terminal velocity (Young & Freedman, 2014). The differential equations for calculating the acceleration of the droplet in x and y-direction are obtained, as shown in Equations 8 and 9 (Dehghani-Sanij et al., 2018).

The droplet velocity in the x-direction dx/dt and y-direction $/dt$, equals u_x and u_y, respectively. Further, the velocity of ambient air in the x and y-direction is represented by u_{rx} and u_{ry}. d represents the droplet diameter.
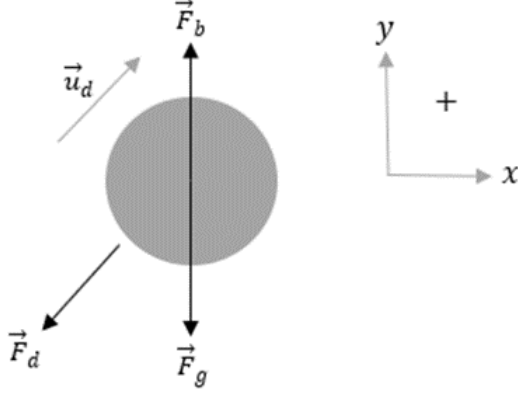
Figure 3. Free body diagram of a water droplet.

$$\frac{d^2x}{dt^2} = -\frac{3}{4}\frac{C_d}{d}\frac{\rho_{amb}}{\rho_d}\left(\frac{dx}{dt} - u_{rx}\right)$$
$$\cdot \sqrt{\left(\frac{dx}{dt} - u_{rx}\right)^2 + \left(\frac{dy}{dt} - u_{ry}\right)^2} \qquad (8)$$

$$\frac{d^2y}{dt^2} = g\left(\frac{\rho_{amb}}{\rho_d} - 1\right) - \frac{3}{4}\frac{C_d}{d}\frac{\rho_{amb}}{\rho_d}\left(\frac{dy}{dt} - u_{ry}\right)$$
$$\cdot \sqrt{\left(\frac{dx}{dt} - u_{rx}\right)^2 + \left(\frac{dy}{dt} - u_{ry}\right)^2} \qquad (9)$$

In this paper, the air represents a mixture of entrained air from the surroundings and air from the nozzle. This is simplified by adding an initial ambient air velocity. The droplet velocity is then calculated by using Equation 10 (Dehghani-Sanij et al., 2018).

$$u_d = \sqrt{u_x{}^2 + u_y{}^2} \qquad (10)$$

To determine the drag coefficient C_d, which is a function of the droplet Reynolds number Re_d, the Schiller Neumann model is applied similar to Dehghani-Sanij et al. (2018):

$$C_d = \begin{cases} \dfrac{24}{\text{Re}_d} & Re_d \leq 1 \\ \dfrac{24}{\text{Re}_d}(1 + 0.15\text{Re}_d^{0.687}) & 1 < Re_d \leq 1000 \\ 0.44 & Re_d > 1000 \end{cases} \qquad (11)$$

$$Re_d = \frac{\rho_{amb}d u_{eff}}{\mu_a} \qquad (12)$$

where u_{eff} is the relative motion of the droplets to the ambient air and μ_a is the dynamic viscosity of air.

2.1.2 Heat transfer

When the droplets are discharged from the nozzle, the heat transfer influences the droplet size. In this model,

convection and evaporation are considered, while conduction and radiation are neglected. It is assumed that the droplet evaporated from positive centigrade until it obtains 0°C. When this temperature is reached, the droplets are considered to be frozen at 0°C.

The following expression is used to calculate the change of the droplet temperature, given in Dehghani-Sanij et al. (2018) as:

$$\frac{dT_d}{dt} = \left[\frac{6(\frac{dm_d}{dt})}{\pi\rho_d d^3}\right]T_d - \frac{6}{\rho_d c_{p,d} d}(Q_e + Q_c) \qquad (13)$$

where the convective heat loss can be found in Lozowski et al. (2000) using

$$Q_c = h_c(T_d - T_{amb}). \qquad (14)$$

The heat transfer coefficient h_c is modeled as

$$h_c = \frac{Nu \cdot k_a}{d} \qquad (15)$$

with the Nusselt number Nu and the thermal conductivity of air k_a.

$$Nu = 2.0 + 0.6Pr^{0.33}Re_d^{0.5} \qquad (16)$$

$$k_a = 9.027 \cdot 10^{-5}\, T_{amb} + 0.0246 \qquad (17)$$

The Prandtl number Pr is modeled like Bergman et al. (2011) using the dynamic viscosity of air μ_a and the thermal diffusivity α_a of air.

$$Pr = \frac{\mu_a}{\rho_{amb} \cdot \alpha_a} \qquad (18)$$

$$\mu_a = \mu_0\left[\frac{T_0 + 120}{T_{amb} + 120}\left(\frac{T_{amb}}{T_o}\right)^{1.5}\right] \qquad (19)$$

$$\alpha_a = \frac{1}{57736 - 585.78\, T_{amb}} \qquad (20)$$

2.1.3 Mass transfer

From Equation 13 Q_e is used. This is the heat loss due to vaporization (Bergman et al., 2011) and is modeled as:

$$Q_e = h_c\left(\frac{Pr}{Sc}\right)^{0.63}\frac{E \cdot \Delta H_{vap}}{P \cdot c_{p,amb}}P_v \qquad (21)$$

where

$$Sc = \frac{\mu_a}{\rho_{amb}D_{d,amb}} \qquad (22)$$

E is the ratio of molar weight, ΔH_{vap} is the heat of vaporization, and $D_{d,amb}$ is the binary diffusion coefficient of water into the air at atmospheric pressure (Incropera, 2017)

$$D_{d,amb} = 0.26x10^{-4}\left(\frac{T_{amb} + 273.15}{273.15}\right)^{1,5} \qquad (23)$$

The heat capacities for the airflow water and entrained air are assumed constant throughout the process. The change of the droplet diameter is calculated by using Equation 24.

$$\frac{dd}{dt} = -\frac{(\frac{dm_d}{dt})}{\rho_d \pi d^2} \qquad (24)$$

where $(\frac{dm_d}{dt})$ is calculated according to Horjen (2013) using:

$$\left(\frac{dm_d}{dt}\right) = \frac{Q_e}{\Delta H_{vap}} A_d \qquad (25)$$

A_d is the surface area of the droplet.

2.1.4 Constants

The constants for the modeling are summarized in Table 1 where the reference is indicated.

Table 1. The table presents constants and initial conditions are used in the model.

	Value	Units	References
$c_{p,amb}$	1.005	[J/kg K]	Cengel et al. (2015)
$c_{p,d}$	4180	[J/kg K]	Cengel et al. (2015)
$d_{annular}$	$1.4 \cdot 10^{-2}$	[m]	Measured
E	0.6215	[-]	(Dehghani-Sanij et al., 2018)
g	9.81	$[m/s^2]$	Cengel et al. (2015)
ΔH_{vap}	$22.6 \cdot 10^5$	$[J/kg]$	Cengel et al. (2015)
P	101325	$[Pa]$	Cengel et al. (2015)
R_a	287	[J/kg K]	Cengel et al. (2015)
$RH\%$	79	$[-]$	Measured
T_{amb}	-3	$[°C]$	Measured
T_o	296.16	$[K]$	(Dehghani-Sanij et al., 2018)
γ	1.4	[-]	Cengel et al. (2015)
ϵ	50	[μm]	Measured
μ_0	$1.8325 \cdot 10^{-5}$	$[Pa \cdot s]$	(Dehghani-Sanij et al., 2018)
ρ_d	1000	$[Kg/m^3]$	Cengel et al. (2015)
Initial conditions			
x_0	0	$[m]$	Defined
y_0	1.324	$[m]$	Measured
u_{rx}	1.0	[m/s]	Defined
u_{ry}	0	[m/s]	Defined
θ	50	[°]	Measured
$T_{d,0}$	1	$[°C]$	Measured
$T_{a,0}$	-37.19	$[°C]$	Nordbø (2021)
d_0	40,50,120,170,360	[μm]	Defined
t	6	$[s]$	Defined

2.2 Experimental setup

Nedsnødd AS is using a transportable snow-producing rig on a car trailer. In short, the rig contained two aggregates, a water tank, a pump, a compressor, an electric converter, a dryer, water, and air hoses, sensors, lance, and a nozzle. The experimental rig is described in detail in Nordbø (2021).

The experimental measurement intends to compare and adjust the model. The model demands an input on bulk flow velocity, droplet sizes, and droplet velocity distribution.

The measurements were performed using a LED-based shadow imaging technique developed in the work by Lundberg et al. (2019). Back-illuminated images were captured by a high-speed camera where the droplets were manually counted by mouse-clicking on the image. The velocity was found from the adjacent frame. The same procedure was performed for 77 droplets used in the experimental measurements. The camera settings are shown in Table 2.

Table 2. High-speed camera settings.

Fastcam – APX RS model 250K	
Frame rate	5000 fps
Shutter velocity	1/50000 sec
Resolution	512 x 1024
Recording time	0.1144 sec

3 Results and discussion

3.1 Experimental

The model developed in this work is based on three experiments (Porsgrunn, Arabygdi, and Kviteseid). The only experiment yielding snow is the Arabygdi experiment. The ambient conditions and the pressure parameters in each experiment are given in Table 3.

The experimental measurement in Arabygdi gives the droplet size distribution in Figure 4 compared to a Rosin-Rammler distribution (solid line). Figure 5 shows the quality of the fit in an ln-ln plot. The fit does not represent the largest droplets very well and can benefit from a higher number of samples. It is important to consider that this is from a single location in the flow and might be different in other locations. The location in the spray is 41 cm from the nozzle and 16 cm radially.

Table 3. Experimental parameters.

Place	*Porsgrunn*	*Arabygdi*	*Kviteseid*
Date	13.03.2021	18-19.03.21	21.03.2021
Altitude	7 m	687 m	307 m
T-Ambient	-2.6 °C	-2.5 to -4 °C	-1 to 1 °C
RH%	96%	79 %	64 %
U-wind	0-0.8 m/s	0-1.7 m/s	5 m/s
P-Water	2.66 bar(g)	4.64 bar(g)	4.64 bar(g)
T-Water	~10 °C	1 °C	2 °C
P-Air	5.38 bar(g)	1.95 bar(g)	1.95 bar(g)
T-Air	10 °C	10 °C	10 °C
T-Wet-bulb	-3.05 °C	- 4.6 °C	-3.64 °C
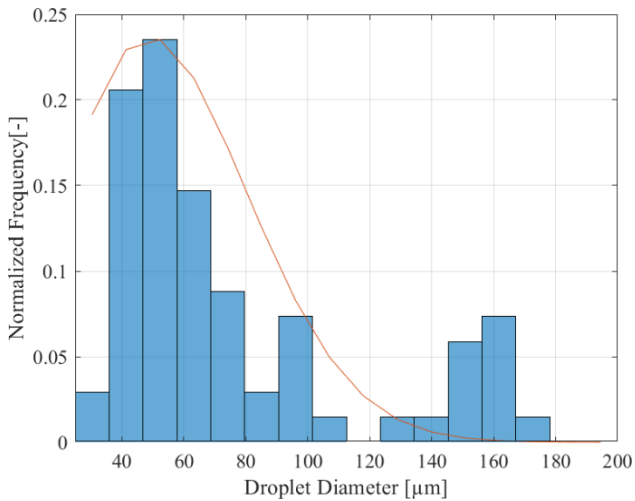
Figure 4. Droplet distribution of experiments in Arabygdi compared to an optimized Rosin-Rammler distribution.
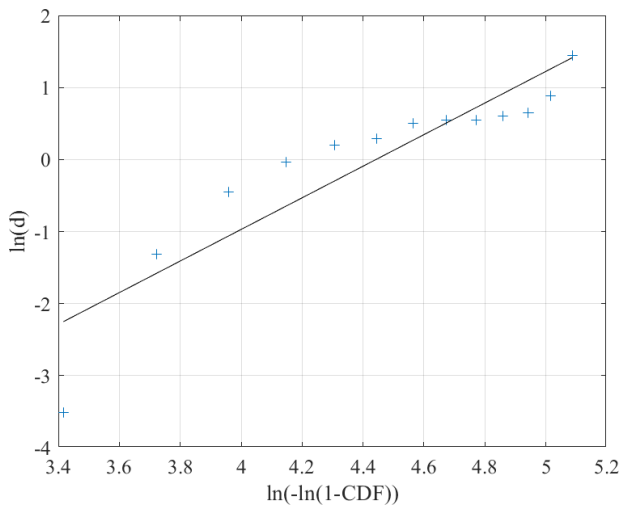
Figure 5. ln-ln plot of the quality of fit for the experiment in Arabygdi, where CDF is the cumulative distribution function.
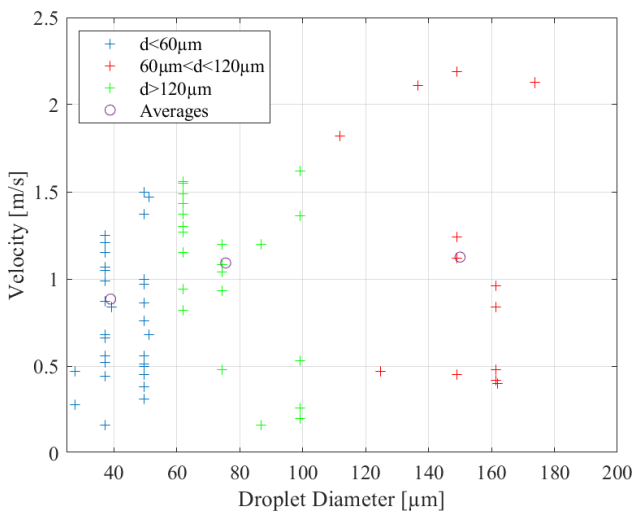
Figure 6. The velocity of the droplets from the experiment in Arabygdi.

The velocity of the droplets (Figure 6) shows a weak tendency of increased velocity with increasing diameter.

Nevertheless, the measurements show that the bulk velocity is approximately constant in this region of the spray.

Visual considerations during the experiment confirmed that the nozzle produced artificial snow at given parameters. From the image shown in Figure 7, the droplets form large agglomerates according to theory.

Figure 7. Rime-shaped snow in Arabygdi.

3.2 Simulation

The trajectory, flight time, velocity- and temperature profile using the initial conditions are shown for droplets with the diameter of 40, 50, 120, 170, and 360 μm. The range of 40 – 170 μm droplet sizes is defined based on the image processing performed in Arabygdi. The 360 μm is to investigate how larger droplets influence heat and mass transfer.

The initial angle of the droplet angle is set to 50°. Also, the initial height of the droplets is defined as 1.324 m, based on the nozzle position measured during the experiment.

The droplets of 40 μm and 50 μm obtain the most significant displacement with more or less neutral gravitational force. The droplet of 360 μm shows weak affection of the entrapped air velocity following a ballistic pattern. The 360 μm droplet shows a higher influence of the gravitational force while the other droplets are drag force driven. This is shown in Figure 8 and Figure 9. The velocity profile of each droplet is shown in Figure 10.

The initial temperature of the droplets is 1 °C based on experimental measurements. The droplets are cooled down to 0 °C within microseconds due to evaporation before the temperature is further decreased. Figure 11 shows how the temperature of the droplets converges to its final temperature.

Figure 11 shows that the 360 μm droplet does not reach the same final temperature as the other droplets. All droplets, except the 360 μm droplet, cool down to a temperature just below the ambient temperature of - 3°C before hitting the ground. The droplet temperature as a function of travel length is illustrated in Figure 11.
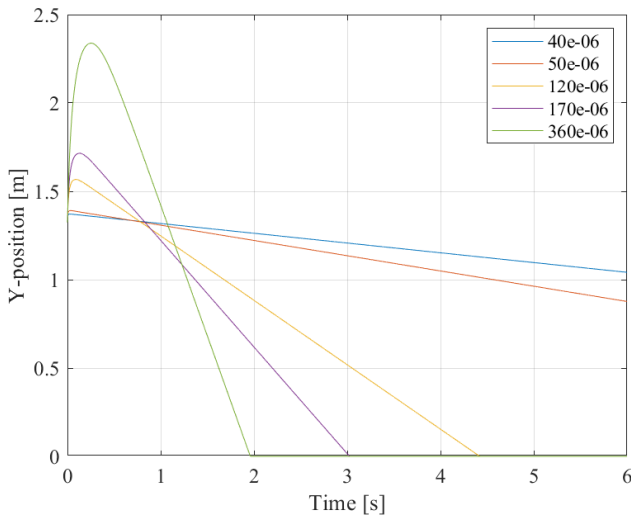
Figure 8. Predicted flight time that is obtained by the modeled droplets.
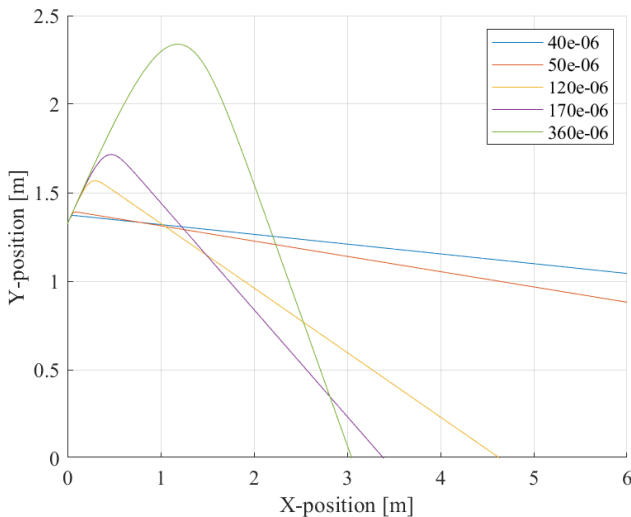
Figure 9. Position/trajectory of the modeled droplets.
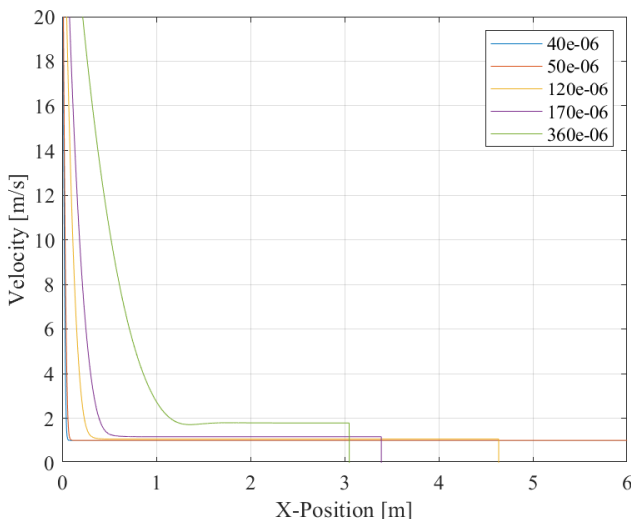
Figure 10. Velocity profile of the modeled droplets concerning the x-position of the droplets.
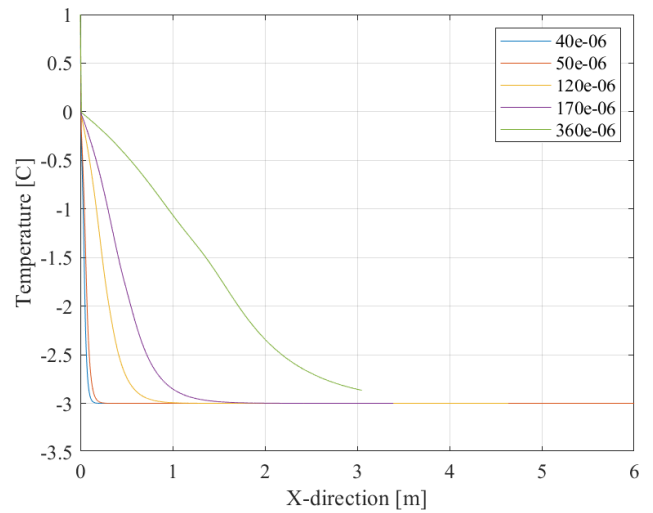
Figure 11. Temperature change concerning the motion of modeled droplets in the x-direction.

The airflow temperature inside the nozzle's throat was calculated to be -37.19 °C, assuming an isentropic process, compressible gas, and the stagnation temperature from the compressor to be 10°C. A thermographic photo captured in Arabygdi shows that the material at the nozzle tip is - 37.5°C, which indicates this to be a reasonable assumption. On the other hand, the amount of water flow was three times greater than the airflow through the nozzle, and the water was assumed to be 1 °C. The heat transfer of the water contributes more significantly to the mixture temperature of the ejected droplets.

A thermographic photograph of the discharged water sheet, 1 cm out from the nozzles exit plane in Arabygdi, indicated that the water was reduced to roughly -1.4 °C. The temperature simulation of the droplets showed that the droplets rapidly decreased at this point of the nozzle. As the thermographic camera used has an accuracy of ± 2°, the result seems reasonable. In addition, the temperature simulation showed that all droplets reached 0 °C within 150 μs and could freeze before they reached the ground. Here, the definition of evaporative heat loss comes into sight. It was defined to stop when the surface temperature of the droplets had reached 0°C. Thus, the water molecules of high internal energy would stop ejecting themselves from the droplets and thereby stabilize the temperature of the droplets. The wet-bulb temperature, measured to be –4.6 °C by using the weather conditions in Arabygdi, was thereby not reached.

Changes in the relative humidity RH% were not simulated in this work. As an effect of this, the evaporative heat transfer was expected to be larger than in the experiment. In the experiments, the humidity from the evaporation is expected to saturate the air rapidly after the atomization.

The diameter 40 and 360 droplets were reduced by 0.04 and 0.06 %, respectively. The experiment in Arabygdi gave snow density of 490 kg/m^3 in the other

locations, no snow was produced. There may have been other factors that influenced the product. The experiment in Porsgrunn was not performed within a continuous cold period like the experiment performed in Arabygdi. Thus, the ground in Porsgrunn was probably not frozen and heated the falling droplets.

The snow shape obtained in Arabygdi was photographed. From the picture, frozen droplets are stacked on each other and may be characterized as rime formation.

4 Conclusion

This work aimed to perform both literature, modeling, and experimental study of artificial snow production in marginal geographic conditions. A snow-producing rig designed by Nedsnødd AS was used during the experimental study. The innovative part of the rig was the assembled novel twin-fluid annular sheet nozzle, where a thin sheet of water was atomized into droplets by high-velocity air.

As the literature on artificial snow production was limited, the water cycle and natural snow formation were studied to understand artificial snow production. A theoretical model was developed to analyze the trajectory and heat and mass balance of a single droplet discharged from the nozzle. The snow density goal was defined to be 500 kg/m3. A high-speed camera was used to record the droplet size and velocity in the spray. The experimental measurements were further used to improve the droplet model.

Only one of the experiments performed in Arabygdi yielded snow with a density of 490 kg/m3, which satisfied the snow density goal of 500 kg/m3.

The model developed during this work can be used for general trends in artificial snow production. The model gives reasonable results for single droplets that can be further developed into a multi-droplet system.

Acknowledgments

References

M. Bellis. Who Invented the Snowmaking Machine? ThoughtCo, Oct. 29, 2020.

O.E.H. Berg, *Optimal produksjon av snø fra flere produksjonsenheter i samme område*. Master's thesis, Department of Engineering cybernetics, Norwegian University of Science and Technology, Trondheim, 2017.

T.L. Bergman, A.S. Lavine, F.P. Incropera and D.P. DeWitt. *Introduction to Heat Transfer, 6th ed*. John Wiley & Sons, Inc, 2011.

Y. A. Cengel, M. A. Boles and M. Kanoglu. *Thermodynamics: An Engineering Approach, 8th ed*. New York: McGraw-Hill Education, 2015.

A.R. Dehghani-Sanij, Y.S. Muzychka and G.F Naterer. Droplet trajectory and thermal analysis of impinging saline spray flow on marine platforms in cold seas and ocean regions. *Ocean Engineering*, 148:538-547, 2018. doi:10.1016/j.oceaneng.2017.11.053.

I. Horjen. Numerical modeling of two-dimensional sea spray icing on vessel-mounted cylinders. *Cold Regions Science and Technology* 93:20–35, 2013. doi:10.1016/j.coldregions.2013.05.003.

F. P. Incropera, D. P. Dewitt, T.L. Bergman and A. S. Lavine. *Incroperas's principles of heat and mass transfer, 1st ed.* New York: John Wiley & Sons Inc, 2017.

E.P. Lozowski, K. Szilder and L. Makkonen. Computer simulation of marine ice accretion. *Philosophical Transactions of the Royal Society A,* 358:2811–2845, 2000. doi:10.1098/rsta.2000.0687.

J. Lundberg, K. Vaagsaether and O.I. Lindløv. Performance of a novel diesel atomization nozzle. Nordic Flame days 2019, August 28th-29th, Turku, Finland, 2019.

M. Nordbø. *Experimental investigation of artificial snow production in marginal geographic conditions*, Master's Thesis, Faculty of Technology, Natural sciences and Maritime Sciences, University of South-Eastern Norway, Norway, 2021.

M. Olefs, A. Fischer and J.Lang. Boundary Conditions for Artificial Snow Production in the Austrian Alps. *Journal of applied meteorology and climatology*, 49(6):1096-1113, 2010. doi:10.1175/2010JAMC2251.1.

Techno Alpin. TT10: Tower power. technoalpin.com (accessed online Apr. 21, 2021).

C.R. Tracy, W.R. Welch and W.P. Porter. *Properties of Air, a Manual for Use in Biophysical Ecology*. Technical report No. 1, third ed. University of Wisconsin, 1980.

J. Xu, Q. Wei, S.Peng and Y. Yu. Error of Saturation Vapor Pressure Calculated by Different Formulas and Its Effect on Calculation of Reference Evapotranspiration in High Latitude Cold Region. *Procedia Engineering*, 28:43-48, 2012. doi:10.1016/j.proeng.2012.01.680.

H. D. Young and R. A. Freedman. *Sears and Zemansky's University Physics with Modern Physics*, 13th Edition, Pearson, 2014.